Effect of Carbon Partitioning and Residual Compressive Stresses on the Lattice Strains of Retained Austenite During Quenching and Isothermal Bainitic Holding in a High Silicon Medium Carbon Steel

S. Pashangeh[1], S. S. Ghasemi Banadkouki[1]*, M.C. Somani[2], J. Kömi[2]

[1]Department of Mining and Metallurgical Engineering, Yazd University, University Blvd, Safayieh, Yazd, PO Box: 98195 – 741, Iran; pashangeh.a@gmail.com (S.P.); sghasemi@yazd.ac.ir (S.S.G.B.)

[2]University of Oulu, Materials and Mechanical Engineering, Centre for Advanced Steels Research, Post Box 4200, 90014 Oulu, Finland; mahesh.somani@oulu.fi (M.C.S.); jukka.komi@oulu.fi (J.K.)

(*Corresponding address: sghasemi@yazd.ac.ir (Tel.:+98913 351 6649))

This article has been accepted for publication and undergone full peer review but has not been through the copyediting, typesetting, pagination and proofreading process, which may cite this article as lead to differences between this version and the Version of Record. Please doi: 10.1002/srin.202100463.

Abstract

The residual compressive stresses and dimensional changes related to the lattice strains of retained austenite (RA) phase in a high-Si, medium-carbon steel (Fe-0.53C-1.67Si-0.72Mn-0.12Cr) were investigated for samples austenitized and quenched for isothermal bainitic transformation (Q&B) in the range 5 s to 1 h at 350 °C. Also, samples were directly quenched in water (DWQ) from the austenitization temperature for comparison with Q&B samples. Field emission scanning electron microscopy combined with electron backscatter diffraction analyses, and X-ray diffraction were employed to investigate the microstructural evolution, phase distribution, and lattice parameters of RA phase. While the Q&B samples showed formation of bainite and also high-carbon fresh martensite in conjunction with stabilization of various fractions of RA, the DWQ samples displayed nearly complete martensitic microstructure. For short holding durations at 350 °C (<< 200 s), there was limited formation of bainite and hence, the inadequate carbon partitioning to the adjacent untransformed austenite areas resulted in significant martensite formation and the associated c/a ratio of martensite resulted in high compressive residual stresses within the RA phase. While, at long isothermal holding times (>> 200 s), there was a significant formation of bainite. In comparison, the DWQ samples displayed maximum lattice strain in a small fraction of untransformed RA phase.

Keywords: quenching and bainitic holding, bainite, martensite, retained austenite, lattice strain.

1- Introduction

The advancements in materials science and engineering have allowed researchers to play with the various phases, properties, and compositions of materials such that the materials can often be tailor-made with the desired properties [1–3]. In steel industries, researchers working on the development of tough, ultrahigh strength steels are regularly focusing on processing schedules involving isothermal holding around the martensite start temperature (M_s), which result in the evolution of complex multiphase microstructures comprising a mixture of bainite, martensite, and retained austenite (RA) with varied size, morphology, and distribution. The RA phase leading to the transformation induced plasticity (TRIP) effect in these advanced multiphase steels contributes to the improved tensile ductility with a concomitant increase in tensile strength [4–7].

The latest development of ultrahigh strength steels has adapted to the new concept of microstructural design involving multiphase, and multi-scale microconstituents [8–10]. In the last

decade, a few novel heat treatment processes, such as quenching and partitioning (Q&P) [11–13], quenching-partitioning-tempering (Q-P-T) [14], and low-temperature bainitic transformation (close to or even below M_s temperature) [15–17], have been designed to achieve an excellent combination of high/ultrahigh strength combined with good low temperature toughness and reasonable ductility. The volume fractions of different microstructural constituents, such as ferrite, bainite, martensite, and retained austenite, determine the final mechanical properties in these groups of advanced high strength steels (AHSS) [18–20]. Depending on the alloy type, chemical composition, and parameters of these novel heat treatment processes, such as the reaustenitization temperature, quenching rate, final quench stop temperature to enable isothermal bainitic transformation and/or carbon partitioning, the heat treated steel samples may contain varied amounts of RA, which can impart a wide range of properties in the end products [3,21–28]. In these novel steel concepts, the role of RA is very complicated depending on the high complexity of the multiphase structures and often has beneficial effects, but at times can have some negative effects on certain properties. Thus, the detection and estimation of retained austenite in respect of its amount, size, distribution, morphology, and stability are considered as key factors in designing the process schedules and assessment of corresponding properties for particular applications [27,29–33].

There are different experimental methods, such as X-ray diffraction (XRD), for investigating the microstructural evolution during (*in situ*) or following (*ex situ*) different heat treatment cycles to exclude the role of specific parameters that may influence the final properties. Crystal size, morphology, and strain distribution also play an important role in the final properties and depend on the processing schedule [34]. Any deviation from the perfect condition is the reason for the broadening of diffraction peaks in the XRD patterns of materials. The lattice strain is the main property that can be extracted from the peak width analysis and is a measure of the disorder in the lattice unit cells arising from crystal imperfections, such as lattice dislocations [35]. X-ray line broadening technique has routinely been used for the investigation of dislocation distribution. For instance, the X-ray peak profile analysis (XPPA) is used to estimate the microstructural quantities including defects and correlate with the observed properties of heat treated or processed materials. XPPA is a simple, but powerful tool to estimate the crystallite size and lattice strain parameters [36]. The lattice strain affects the Bragg peak in different ways such as increasing the peak width and peak intensity and shifting the peak position of the 2θ angle accordingly, where θ is the Bragg angle. There are several methods reported in the literature to estimate the crystallite size and lattice strain, such as the pseudo-Voigt function, Rietveld refinement, and Warren-Averbach analyses [37–39]. However, the Williamson–Hall (W–H) analysis is a simplified integral breadth method used for estimating the crystallite size and also the lattice strain, where both size-induced and strain-induced broadening are deconvoluted by employing the peak width as a function of 2θ [40]. Depending on

different θ positions, the separation of size and strain broadening analysis is done using W–H analysis [41,42]. According to this method, strain varies as tanθ from the peak width [41]. The size and strain effects on peak broadening are known from the above difference of 2θ.

Due to less attention paid on studying the details of lattice strain distribution in the RA phase and also its importance in structural evolution of AHSSs, this research work has been undertaken to estimate the microstructural quantities such as lattice strain determination of RA phase using the W-H analyses of XRD data measurements made on a high-silicon medium carbon steel samples (DIN 1.5025), isothermally held slightly above the M_s temperature in comparison to those quenched directly to room temperature from the austenitization temperature. The results were correlated to the microstructural evolutions in different heat treatment conditions characterized by FE-SEM examination combined with EBSD analyses.

2- Materials and experimental process

A medium-carbon commercial grade (DIN1.5025) steel sheet of thickness 1 mm was chosen for this study and its chemical composition is given in Table 1. The silicon content of 1.670 wt.% was useful due to its effectiveness in preventing (or at least delaying) carbide precipitation and growth during isothermal decomposition of austenite and hence promoting the partitioning of carbon to the adjacent untransformed austenite areas, thus facilitating stabilization of a part or whole of the carbon-enriched austenite. Mn, a strong austenite former, was somewhat lower than desired for enhanced austenite stabilization during carbon partitioning. The critical temperatures of the phase transformations were determined by conducting dilatometry tests in a Gleeble simulator at the heating and cooling rates of 0.2 °C/s and 150 °C/s, respectively, and the corresponding results are given in Table 2. Samples of the dimensions 30× 30× 1 mm were cut from the as-received strip sample for carrying out the heat treatments, which were done in two steps. First, the proposed samples were heated at 900 °C for 5 min in an electrical resistance furnace and then air-cooled to room temperature in order to exclude previous processing history and develop fine-grained martensitic microstructures with the possibility of grain refinement during reaustenitization in the subsequent step. Accordingly, in the second step, the samples were reaustenitized at 900 ºC for 5 min prior to quenching and bainitic holding (Q&B) in a salt bath maintained at 350 ºC, which is above the M_s temperature (275 °C, see Table 2), and then held for different durations between 5 s to 1 h (five different holding times including 5 s, 30 s, 200 s, 600 s, and 1 h) to facilitate bainitic transformation. The Q&B samples were finally quenched in water to room temperature. Besides, a number of samples (3 samples for the accuracy of results) were directly quenched in water (DWQ) following reaustenitization at 900 ºC for 5 minutes for favor of detailed comparison with the Q&B

samples in respect of microstructural quantities (Figure 1). The heat treatment cycles were so designed in order to be able to unravel the effects of different parameters including lattice strain, carbon partitioning, martensite phase transformation, and residual compressive stresses on the lattice unit cell of the austenite phase.

To investigate the microstructural features, the heat treated samples were mounted, ground, and polished according to ASTM E3-01 standard. The samples were etched in a 2% Nital solution (2mm HNO_3 in 98 mm ethanol) for further microstructural observations and phase identification using an FE-SEM model Zeiss Ultra Plus equipped with an EBSD facility. The volume fraction and mean carbon content of the retained austenite in the specimens were determined by XRD using a Rigaku SmartLab 9 kW equipment. The measurements were performed by using a CoK_α radiation source at 135 mA and 40 kV conditions with 2θ ranging between 45 and 130° and the rotation performed at 7.2 °/min. The volume fraction and also the lattice parameter of the RA phase were measured using a direct comparison approach, comparing the integrated intensities of (111), (200), (220), and (311) of FCC diffracted planes with (101), (002), (112) and (202) of BCC planes, respectively [43]. The carbon content was determined by using the relationship [43]:

$$a_\gamma\,[^oA] = 3.572 + 0.033x_C + 0.0012x_{Mn} + 0.0056x_{Al} + 0.00157x_{Si} \quad \text{Equation (1)}$$

where a_γ is the lattice parameter of the austenite in angstroms (Å) and x_C, x_{Mn}, x_{Al}, x_{Si} are the concentrations in weight percent of carbon, manganese, aluminum, and silicon, respectively. Also, the lattice strain and lattice parameter of RA phase were estimated by using the XRD results according to the W–H method [41,42], as clarified in Equation 2,

$$\beta_{hkl}\cos\theta = K\lambda/D + 4\varepsilon\sin\theta \quad \text{Equation (2)}$$

where, β_{hkl} = instrumental broadening, D = crystallite size, K = shape factor (0.9), λ = wavelength of Co-k_α radiation (1.789 A°), θ = Bragg angle and ε = lattice strain. Referring to Equation (1), a graph is plotted with 4sinθ considered along the x-axis and $\beta_{hkl}\cos\theta$ along the y-axis for plotting the experimental data from different heat treatment conditions. From the linear fit to the data, the crystallite size was estimated using the intercept on the y-axis and the lattice strain ε from the slope of the fit.

Table 1- Chemical composition of the investigated high silicon medium carbon steel

Elements	**C**	**Si**	**Mn**	**Cr**	**S**	**P**	**Fe**
wt.%	0.529	1.670	0.721	0.120	0.023	0.022	Balance

Table 2- Critical temperatures achieved from dilatometry analysis of the investigated high silicon medium carbon steel

Critical Temperature	A_{c1}	A_{c3}	M_s
(°C)	765	835	275

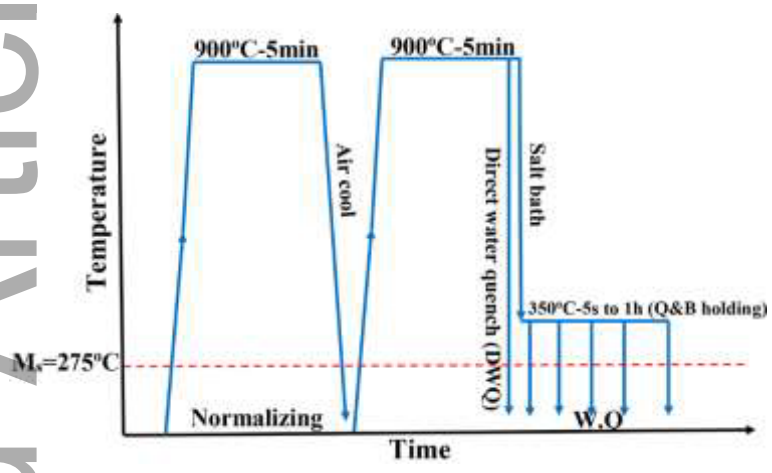

Figure 1- A schematic of the 2-step heat treatment cycle, showing the experimental details of the samples after quenching and bainitic (Q&B) holding (5 s, 30 s, 200 s, 600 s, and 1 h) and direct water quenching (DWQ).

3- Results and discussion

3-1- Microstructural features

Typical examples of representative microstructures of the specimens isothermally held at 350 °C (above the M_s temperature (≈ 275 °C)) for different durations in comparison to that of the DWQ samples, as recorded by FE-SEM, are presented in Figure 2. The presence of only a few bainitic laths indicates that the formation of bainite has just begun at about 5 s (Figure 2-a), as the microstructure is essentially martensitic with a small fraction of very fine austenite, though difficult to discern from the microstructure (but confirmed by XRD, as described later). By increasing the isothermal holding time at 350 °C, bainite formation progresses further and in about 200 s, the structure is essentially a combination of bainite, fresh martensite, and some retained austenite (Figure 2-b). As illustrated in the high magnification in-lens electron image at the top right-hand micrograph in Figure 2-b, the bainitic phase has formed and grown from the prior austenite grain boundaries (PAGB). Also, the islands of both martensite and RA microconstituents (M/RA) have

been revealed in the microstructure (Figure 2-b), as the time for carbon partitioning from bainitic ferrite to the adjacent prior austenite was inadequate to equilibrate carbon in the austenite. Hence, austenite was only partially stabilized down to room temperature, with a good fraction transforming to martensitic laths on final cooling. With further holding to a longer time at 600 s (Figure 2-c), extensive bainite formation has already occurred and was nearly complete in about an hour (Figure 2-d). The corresponding microstructures revealed significant formation of bainitic ferrite along with stabilization of some fractions of finely dispersed RA. These microstructural observations indicated that a complex mixture of multiphase microstructures including bainite, martensite, and RA microphases, were achieved after Q&B heat treatment at 350 ºC. Extensive microstructural examination failed to reveal any carbides at least up to 200 s of holding suggesting that the presence of high silicon (1.67 wt%) in the steel prevented the formation of carbides, despite the presence of significant carbon content in the steel (0.529 wt.% C) and high isothermal transformation temperature (350 °C), thus leading to peak retained austenite content of 18 %, as discussed later. During further holding, the retained austenite fraction decreased significantly beyond 200 s and the carbon enrichment of the austenite slowed down indicating the occurrence of carbide precipitation in the bainitic laths. Besides lath martensite, bainite, and carbon-enriched fine interlath austenite, carbides were also seen in Q&B samples isothermally held for 600 s and 1 h, as reported elsewhere [7]. In comparison, the DWQ samples water-quenched directly to room temperature from 900 ºC resulted in nearly complete transformation to martensite, as shown in Figure 2-e, and the presence of other possible microphases such as untransformed austenite, if any, was impossible to detect and distinguish from the rest of the microstructure.

For further investigation regarding the distribution and morphology of RA phase, EBSD measurements were carried out to reveal the microstructural details. Typical examples of EBSD images (a combination of image quality (IQ) with phase map (PM)) of various Q&B samples are shown in Figure 3. The combined analysis of EBSD images allows distinguishing different sub-areas including martensite in combination with bainitic regions. These EBSD figures can provide better information about the location, distribution, and morphological features of RA in the microstructures. As shown in Figure 3-a for the sample isothermally held for 5 s at 350 ºC, the microstructure essentially depicts a body-centered cubic (BCC) crystal structure (red color region) corresponding mostly to martensite phase (see Figure 3-a), along with a very small amount of RA phase (face-centered cubic (FCC) structure) mostly present as thin films and/or also some blocky shapes in the microstructure (green color). The bainitic areas appear as bright red color in the EBSD images due to the higher confidence indexing of bainitic crystals, thus causing the appearance of bright regions in IQ maps and consequently bright red color in combined PM+IQ maps (Figure 3).

While the martensite has poor confidence indexing of crystallographic intensity caused by the higher intensity of noise due to internal strains and dislocations and hence, these regions appear somewhat darker in comparison to bainite marking poor indexing in the IQ maps, and subsequently as dark red regions in PM+IQ images, Figure 3. This means that the bainitic crystals are generally much better indexed in EBSD images (IQ maps) than that of martensite crystals, which appear relatively darker in contrast (dark red color, i.e, somewhat poorly indexed) in the PM+IQ EBSD images in comparison to the bright red areas of bainite phase. Samples held at 350 ºC for 200 s (Figure 3-b) showed a microstructure comprising of bainite (red color), fresh martensite (FM) (dark red color) and RA (green color) appearing mostly in blocky as well as some interlath morphologies; revealed clearly at a higher magnification. Therefore, by increasing the isothermal holding time at 350 ºC to 200 s, the morphology of RA phase appeared to have a significant fraction of blocky shaped austenite(Figure 3-b) also, besides retaining thin films between bainitic laths due to the enhanced carbon partitioning from bainite to untransformed austenite. Following holding at 350 °C for 200 s, a significant fraction of austenite (more than 20%) was still untransformed and it got extensively enriched with carbon atoms during the process of carbon partitioning. Not all of this austenite was in the form of interlath films, but a significant fraction was present as pools between bainitic packets. A large fraction of this austenite (18 %) was stabilized at room temperature with average carbon content of 1.265 %. Another aspect of the phase distribution is the occurrence of blocky islands of martensite (dark red color) in the BCC structure, surrounded by RA phase (green color). As the isothermal holding was increased up to 1 h at 350 ºC, the bainitic transformation was nearly complete (red color) resulting in a high fraction of the BCC bainitic ferrite, whereas FCC RA phase was distributed as both blocky grains as well as thin films, Figure 3-c. It is to be noted that the formation of a small fraction of martensite (dark red color) can be revealed only in the case of the samples held for 200 s (Figure 3-b) and 1 h (Figure 3-c) at 350 ºC, unlike in the case of the sample isothermally held for 5 s, which was essentially martensitic with only a small fraction of fine RA, as stated earlier (Figure 3-a). The representative EBSD image of DWQ sample, shown in Figure 3-d, shows few blocky grains of RA distributed throughout the martensitic matrix. These microstructural investigations clarify that the RA phase has a varied morphology (both thin film and blocky shapes) and is present not only in Q&B samples, but also DWQ samples.

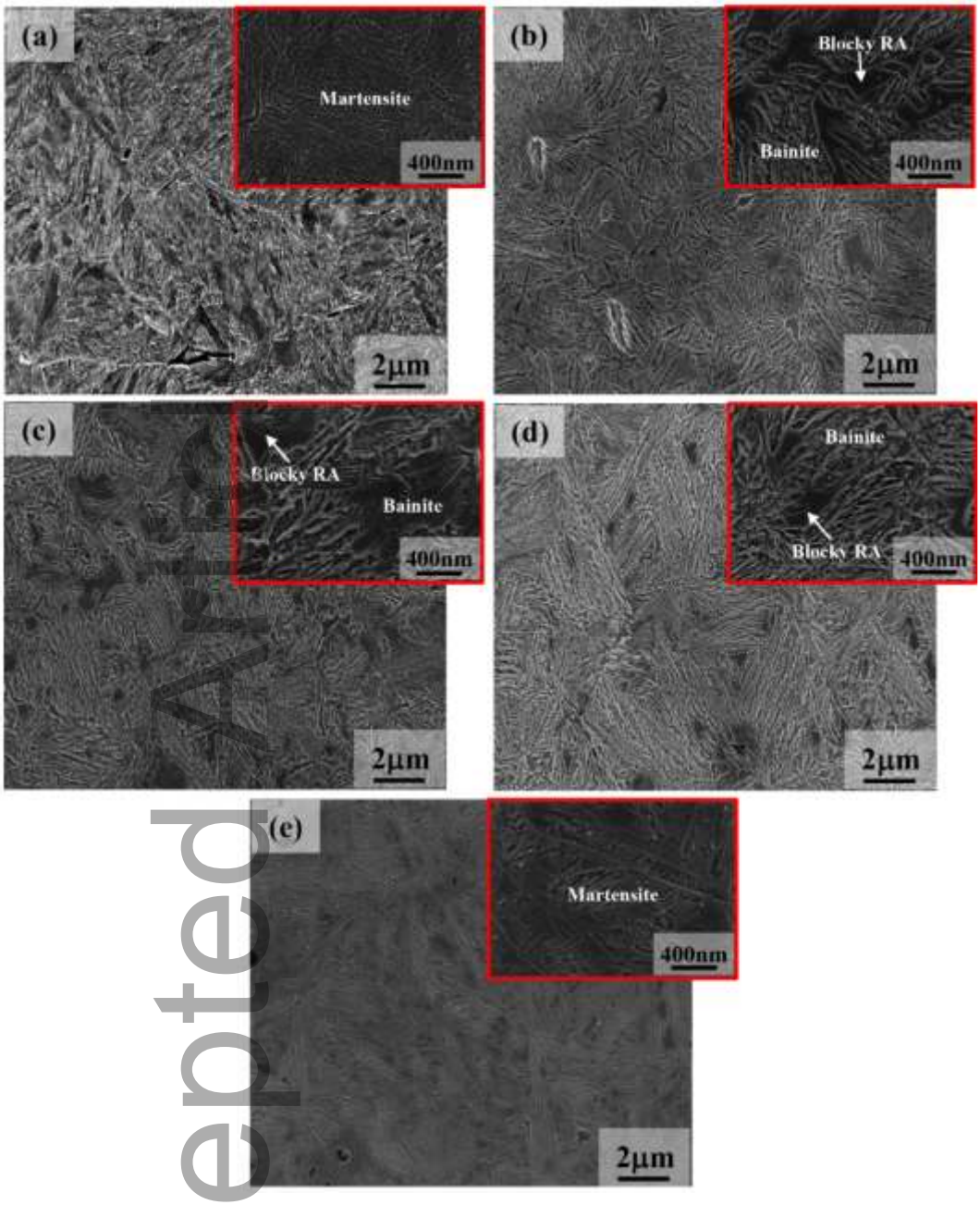

Figure 2- FE-SEM images of different heat treated samples including isothermal holding at 350 ºC for: (a) 5 s; (b)200 s; (c)600 s; (d)1 h; in comparison to (e) DWQ ones.

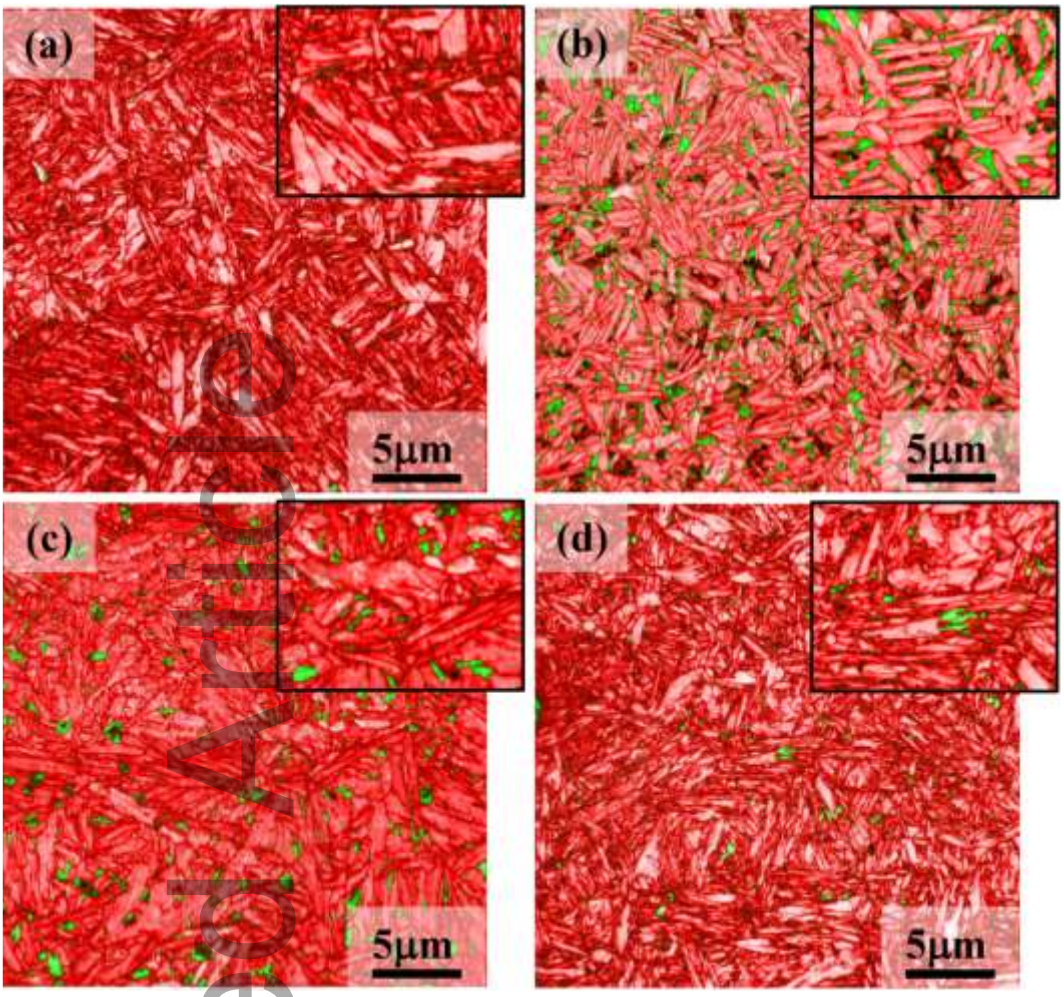

Figure 3- IQ+ PM EBSD images of Q&B samples isothermally held at 350 ºC for: (a) 5 s; (b) 200 s; and (c) 1 h, in comparison with micrograph of (d) DWQ sample. The RA is green, while the bainite and fresh martensite phase constituents are bright red and dark red colored, respectively.

3-2- XRD Analysis of multiphase microstructures

The XRD results of different Q&B samples after isothermal holding for various durations between 5 s to 1 h at 350 ºC in comparison to the DWQ samples are shown in Figure 4. As can be observed, the crystal structures have been broadly characterized in two groups, identified as face-centered cubic (FCC-austenite) and body-centered cubic (BCC-ferrite, bainite, and martensite) microphases. Since the isothermal holding temperature for bainitic transformation is relatively low (350 °C) and the maximum duration of heat treatment is 1 h, it is unlikely that there would have been any significant diffusion and partitioning of substitutional alloying elements (such as Si, Mn, etc.). Hence, only the diffusion and partitioning of carbon have been considered in these calculations. Based on the intensities of the FCC peaks, the RA volume fractions and their carbon concentrations were approximated and the corresponding results are listed in Table 3. A similar carbon concentration calculation method was used earlier with reasonable estimation and has been

presented elsewhere [38]. As can be seen, the volume fraction of RA phase in Q&B samples held at 350 ºC at first increased with isothermal holding time up to 200 s (18 vol.% RA) and then gradually decreased with further holding for long durations, up to 1 h (6.9 vol.% RA), obviously as a consequence of more bainite formation. The corresponding carbon enrichment, however, showed markedly different behavior, as the carbon content increased with holding time up to 1 h in these Q&B heat treated samples, as a result of extensive carbon partitioning from bainitic ferrite to the adjacent untransformed prior austenitic films/grains. Also according to the XRD spectra, displayed in Figure 4, the peaks related to the RA phase with FCC structure are not only broadened owing to the increased strain in the austenite due to the formation of bainite and/or martensite, but also marginally shifted to higher angles as the isothermal holding time was increased from 5 s to 1 h at 350 ºC. This behavior suggests that during phase transformation from prior austenite (with FCC structure) to bainite and/or martensite (BCC/BCT structure), more than 8.8% volume expansion would have occurred resulting in lattice strains in the microstructures, and finally, shifting of diffraction peaks [44]. The EBSD results too revealed the presence of martensite (and also some bainite) in the microstructures of Q&B samples, especially after 5 and 200 s, and indeed, extensive martensite formation in DWQ samples, Figure 3. The enlarged section of XRD patterns (the XRD profiles containing the FCC {111} peak) shown in the top right-hand part of Figure 4 clearly reveals this behavior.

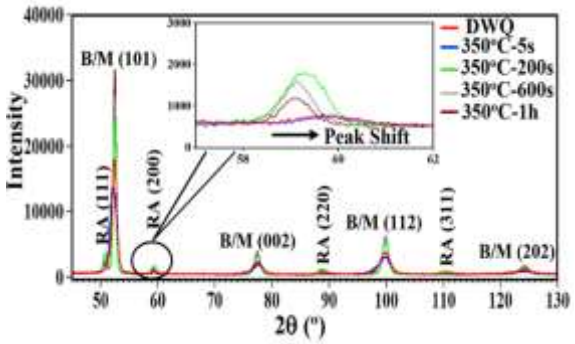

Figure 4- The X-ray diffraction spectra for different Q&B samples. The XRD spectrum of DWQ sample is also included for comparison.

3-3- Carbon partitioning and lattice strain of RA phase

The average carbon content and lattice strain of RA phase determined from the XRD spectra for different heat treatment conditions according to the W-H method is presented in Table 3. The average carbon content of RA increased from 0.6 to 1.39 wt.% with the increase in isothermal holding time from 5 s to 1 h at 350 °C, suggesting the occurrence of effective carbon partitioning during bainitic transformation in Q&B samples, in comparison to the DWQ samples (0.568 wt.%

C), which showed carbon level close to that of the composition of the steel (0.529 wt.%). The carbon content of the RA phase first increased sharply up to about 200 s (1.27 %), beyond which it slowed down significantly at about 600 s (1.36%) with a maximum value estimated after 1 h holding (1.39%). In contrast, the variation in lattice strain showed a slightly different pattern with an increase in isothermal holding time. At first, the lattice strains varied in a narrow range from 0.68 to 0.686 %, as the isothermal holding time was increased from 5 s to 200 s. However, further increase in holding time to 600 s and 3600 s led to a significant drop in lattice strain to 0.557 and 0.408 %, respectively. In comparison, the DWQ samples showed maximum lattice strain in RA phase (0.86 %), as expected. For a better understanding, the variation of average carbon content and lattice strain in the RA phase are graphically shown as a function of isothermal holding time in Figure 5. As is evident, the carbon content of the RA phase increased sharply up to about 200 s, beyond which it reached a plateau at about 600 s (1.36%) with the carbon content remaining practically same with a peak value estimated at 1 h (1.39%). In correspondence, the lattice strain varied in a narrow range up to about 200 s, as mentioned above, obviously as a result of low bainite formation in the beginning (up to 50 s) and hence, significant martensite formation in the multiphase microstructure during final quenching, thus causing high lattice strains. However, at 200 s, significant bainite formation and also carbon partitioning in the microphases caused high lattice strains in RA with little or no stress relaxation, though some martensite may have also formed during final cooling causing additional lattice strains. Martensite formation which contains a relatively high carbon content and the associated c/a ratio of martensite phase resulted in high compressive residual stresses within the RA phase after final water quenching. On the other hand, due to longer holding beyond 200 s, there is an extensive recovery of dislocations in bainite and with practically no martensite forming during subsequent cooling, the lattice strains in RA dropped significantly. Even though the carbon content of the austenite increased slightly with the increase in isothermal holding time beyond 200 s, but it did not cause any significant lattice strains in RA, as the recovery was extensive.

In comparison the DWQ samples showed large lattice strains in the retained austenite due to the formation of a large fraction of nearly untempered martensite, i.e., phase transformation from FCC to BCT lattice, leading to a highly dislocated microstructure and causing extensive strains in the limited RA phase between the martensitic laths. This is in good agreement with the results presented in Table 3 and Figure 5. The occurrence of lattice strains in the RA phase due to the carbon partitioning as well as the volume expansion during phase transformation from FCC to BCT caused the shifting of the diffraction peaks of RA to higher angles. Hence, for the samples with high martensite volume fractions (DWQ), significant micro-strains could be generated within the

RA and correspondingly, a high degree of shift occurred in the diffraction peaks. This strain distribution in the RA phase has a very important effect on the stability of RA phase during tensile testing. For example, higher lattice strains can cause lower mechanical stability of this phase. On the other hand, the presence of defects in the crystal structure, such as lattice strains, does alter the interplanar spacing between the atomic (hkl) planes and in turn causes shifts in the diffraction patterns [45]. The curves presented in Figure 5 revealed that both the carbon partitioning together with residual compressive stresses affected the lattice strains in RA and the optimum conditions were achieved around 200 s isothermal holding as marked by the arrow in Figure 5, which also corresponds to a high RA fraction in the steel with good stability (1.265 wt.% C). At first, by increasing the isothermal holding time at 350 ^{o}C, lattice strain varied in a narrow range up to 200 s and then decreased at 1 h isothermal holding, which is in good agreement with the microstructural observations, Figure 3. This result indicates that both the carbon partitioning as well as residual compressive stresses at first caused enhanced lattice strains, but at long isothermal holding times (typically 600 s and beyond), reduced residual compressive stresses resulted in decreased lattice strains due to extensive bainite formation in conjunction with high stress relaxation.

Table 3- The estimated volume fraction, carbon content, and lattice strain of RA after different heat treatment conditions, as extracted from the XRD spectra presented in Figure 4

Sample Mark	Vol. Fraction of RA (%)	Carbon Content of RA (wt.%)	Lattice Parameter of RA (A^{o})	Lattice Strain of RA (%)
350^{o}C-5s	4.7	0.60	3.590	0.68
350^{o}C-30s	10.9	0.85	3.598	0.62
350^{o}C-200s	18	1.265	3.612	0.686
350^{o}C-600s	12.65	1.356	3.615	0.557
350^{o}C-1h	6.9	1.39	3.616	0.408
DWQ	4.3	0.568	3.589	0.86

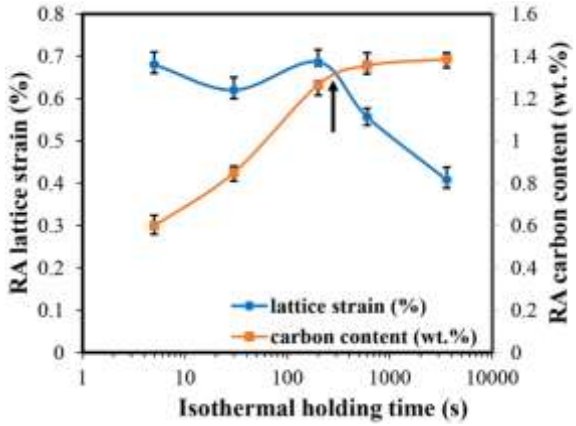

Figure 5- The variation in average carbon content and lattice strain of RA plotted against the isothermal holding time (on a logarithmic scale) for Q&B heat treated samples.

4- Conclusions

In this research work, the effect of isothermal holding time on the lattice strain of RA phase was estimated using W-H analyses of XRD data measured on Q&B samples of a high-silicon medium carbon steel samples (DIN 1.5025), isothermally heat treated slightly above the M_s temperature at 350 ºC in comparison to its DWQ variant, cooled directly to RT following reaustenitization. The results were correlated to the phase constituents, particularly the RA fractions and corresponding carbon contents as a function of hold time. The following results were achieved:

1. The RA phase was distributed in both thin film and blocky shape morphologies in the multiphase microstructures of Q&B heat treated samples in comparison to mostly blocky shape morphology within the martensitic microstructure, though very fine interlath austenite (<100 nm), if any, cannot be detected by EBSD due to limitation of resolution.
2. The volume fraction of RA phase increased to the maximum value of 18 % as a result of increase in isothermal holding time to 200 s at 350 ºC, beyond which it decreased to 12.7 and 6.9 % with a further increase in isothermal holding time to 600 s and 1 h, respectively. This is due to increased bainite formation in the multiphase microstructures as well as loss of carbon due to carbide formation beyond about 200 s isothermal holding.
3. The carbon content of RA phase first increased sharply up to about 200 s (1.27 %), beyond which it stabilized at about 600 s (1.36%) with a maximum value (1.39%) estimated at 1 h holding. The corresponding lattice strain of RA varied in a small range until 200 s and then decreased sharply during further isothermal holding essentially due to extensive recovery of dislocations.

4. The optimized effect of isothermal holding with a high fraction of RA(18%) containing reasonably high carbon content (1.27% C) suggesting good stability occurred at about 200 s, with the only limited restoration of lattice strains (residual compressive stresses).
5. The limited RA(4.3) in DWQ samples has a higher lattice strain in comparison to Q&B heat treated samples, obviously due to the high residual compressive stresses generated in RA as a consequence of a significant fraction of fresh martensite formation during water quenching to room temperature.
6. At low isothermal holding times, limited bainite formed resulting in inadequate carbon partitioning to the adjacent prior austenite films/grains during isothermal holding at 350 ºC and hence transformation of fresh martensite during final cooling led to high lattice strain distribution in the RA phase. On other hand, extensive restoration of compressive stresses due to stress relaxation during long isothermal holding times resulted in an opposite effect on the RA lattice strains, which decreased rapidly beyond about 200 s.

Acknowledgments

The funding of this research activity under the auspices of the Genome of Steel (Profi3) by the Academy of Finland through project #311934 is gratefully acknowledged. S. Pashangeh expresses her gratitude to the Ministry of Science Research and Technology in Iran for funding a research visit to the University of Oulu, Finland to conduct this research work.

Declarations

"The authors declare no conflict of interest."

Data availability

http://dx.doi.org/10.17632/h7mhv9bt8j.1

References:

[1] P. Singh, S. Singh, *Journal of Process Mechanical Engineering,* **2018**, 1–8.

[2] S. Pashangeh, H.R. Karimi Zarchi, S.S. Ghasemi Banadkouki, M. Somani, *Metals*, **2019**, 9, 492.

[3] A. Navarro-López, J. Hidalgo, J. Sietsma, M.J. Santofimia, *Materials Characterization*, **2017**, 128, 248–256.

[4] Y. Onuki, T. Hirano, A. Hoshikawa, S. Sato, *Metallurgical and Materials Transactions A*, **2019**, 50, 4977-4986.

[5] R.W. Wei, L.C. Wang, Y. Xiao, L. Wang, *Acta Metallurgica Sinica (English Letters)*, **2015**, 28, 386-393.

[6] E. De Moor, J.G. Speer, *Automotive Steels*, **2016**, 289-316.

[7] S. Pashangeh, M.C. Somani, S.S. Ghasemi Banadkouki, H.R. Karimi Zarchi, P. Kaikkonen, D.A. Porter, *Materials Characterization*, **2020**, 162, 110224.

[8] H. Dong, *China Technology Science*, **2012**, 55, 1774–1790.

[9] Q. Luo, *Journal of Material Engineering and Performance*, **2016**, 25, 2170–2179.

[10] S. Pashangeh, M. Somani, S.S. Ghasemi Banadkouki, *ISIJ International*, **2021**, 61, 442–451.

[11] D. V. Edmonds, K. He, F.C. Rizzo, B.C. De Cooman, D.K. Matlock, J.G. Speer, *Materials Science and Engineering A*, **2006**, 438–440, 25–34.

[12] H. Kong, Q. Chao, M.H. Cai, E.J. Pavlina, B. Rolfe, P.D. Hodgson, H. Beladi, *Materials Science and Engineering A,* **2017**, 707, 538–547.

[13] J.G. Speer, F.C.R. Assunção, D.K. Matlock, D. V. Edmonds, *Materials Research*, **2008**, 8, 417–423.

[14] J. Dong, X. Zhou, Y. Liu, C. Li, C. Liu, H. Li, *Materials Science and Engineering A,* **2017**, 699, 283–293.

[15] F.G. Caballero, H. Bhadeshia, K.J.A. Mawella, D.G. Jones, P. Brown, *Materials Science and Technology*, **2002**, 18, 279–284.

[16] M.J. Peet, Ph.D. thesis (2010).

[17] C. Garcia-Mateo, F.G. Caballero, H.K.D.H. Bhadeshia, *Materials Science Forum*, **2005**, 500-501, 495–502.

[18] P. Eftekharimilani, R.M. Huizenga, B. Kim, A. Bernasconi, M.J.M. Hermans, *Metallurgical and Materials Transactions A*, **2017**, 49, 78–87.

[19] S. Pashangeh, S.S.G. Banadkouki, M.C. Somani, *Journal of Materials Research and Technology*, **2020**, 9, 5007–5023.

[20] A. Contreras, A. López, E.J. Gutiérrez, B. Fernández, A. Salinas, R. Deaquino, A. Bedolla, R. Saldaña, I. Reyes, J. Aguilar, R. Cruz, *Materials Science and Engineering A,* **2020**, 772,138708.

[21] A.H. Nakagawa, G. Thomas, *Metallurgical Transactions A*, **1985**, 16, 831–840.

[22] H. Guo, G. Gao, X. Gui, R.D.K. Misra, B. Bai, *Materials Science and Engineering A,* **2016**, 667, 224–231.

[23] P. Huyghe, L. Malet, M. Caruso, C. Georges, S. Godet, *Materials Science and Engineering A,* **2017**, 701-254–263.

[24] S. Yan, X. Liu, W.J. Liu, T. Liang, B. Zhang, L. Liu, Y. Zhao, *Materials Science and Engineering A,* **2017**, 684, 261–269.

[25] S. Pashangeh, M. Somani, S.S. Ghasemi Banadkouki, *Journal of Materials Research and Technology*, **2020**, 9 (3), 3438–3446.

[26] M.J. Santofimia, L. Zhao, R. Petrov, J. Sietsma, *Materials Characterization*, **2008**, 59, 1758–1764.

[27] Z.J. Xie, G. Han, W.H. Zhou, C.Y. Zeng, C.J. Shang, *Materials Characterization,* **2016**, 113, 60–66.

[28] B.V.N. RAO, M.S. RASHID, *Materials Characterization,* **1997**,39, 435–453.

[29] A. Arbor, (1980).

[30] Y. Gotoh, K. Koga, N. Sasaguri, N. Takahashi, *IEEE Transactions on Magnetics*, **2006**, 42, 3180–3182.

[31] L. Zhao, N.H. Van Dijk, E. Brück, J. Sietsma, S. Van Der Zwaag, *Materials Science and Engineering A,* **2001**,313, 145–152.

[32] J.H. Ladriere, X.J. He, *Materials Science and Engineering,* **1986**, 77, 133–138.

[33] A. Mostafapour, A. Ebrahimpour, T. Saeid, *International Journal of ISSI*, **2016**, 13, 1–6.

[34] P.Bindu, S. Thomas, *Journal of Theoretical and Applied Physics*, **2014**, 8, 123–134.

[35] T. Ungár, J. Journal of *Materials Science*, **2007**, 42, 1584–1593.

[36] B.D. Cullity, S.R. Stock, 3rd edition, *Upper Saddle River*, **2001**.

[37] B.E. Warren, B.L. Averbach, *Journal of Applied Physics*, **1950**, 20, 595.

[38] B.Y.D. Balzar, H. Ledbetter, *Journal of Applied Crystallography*, **1993**, 26, 97–103.

[39] S. Koch, R. Centrum, *Acta Crystallographica*, **1967**, 22, 151-152.

[40] C. Suryanarayana, M.G. Norton, *Springer Science & Business Media*, **2013**, 13-19.

[41] Y.T. Prabhu, K.V. Rao, V.S.S. Kumar, B.S. Kumari, W*orld Journal of Nano Science and Engineering*, **2014**, 04, 21–28.

[42] V. Mote, Y. Purushotham, B. Dole, *Journal of Theoretical and Applied Physics*, **2012**, 6.

[43] Amit K. Behera, G.B. Olson, *JOM*, **2019**, 71, 1375-1385.

[44] R. Hossain, F. Pahlevani, M.Z. Quadir, V. Sahajwalla, *Scientific Reports*, **2016**, 6, 1–11.

[45] K. Sandeep, A. Crivoi, M.J. Tan, T. Anna, M. Iulian, *Materials Research Proceedings*, **2016**, 2, 211–216.

The residual compressive stresses and dimensional changes related to the lattice strains of retained austenite (RA) phase in a high-Si, medium-carbon steel investigate for samples after Q&B heat treatment. The results confirm that carbon partitioning to the adjacent untransformed austenite results in significant martensite formation which causes high compressive residual stresses within the RA phase.

S. Pashangeh, S. S. Ghasemi Banadkouki*, M.C. Somani, J. Kömi

Effect of Carbon Partitioning and Residual Compressive Stresses on the Lattice Strains of Retained Austenite During Quenching and Isothermal Bainitic Holding in a High Silicon Medium Carbon Steel